scientific reports

Check for updates

OPEN

Broadband terahertz holography using isotropic VO_2 metasurfaces

Jiayu Zhao, Runxuan Zhang, Sicheng Cao, Mingwei Zhuang✉ & Zhengyong Song✉

Vanadium dioxide (VO_2) exhibits exceptional phase transition characteristics that enable dynamic manipulation of electromagnetic wave. In this study, a novel design of bilayer isotropic metasurface is introduced. It leverages insulating-to-metallic phase transition of VO_2 to enable broadband holography for terahertz wave. For the metallic VO_2, the upper VO_2 antennas reflect incident terahertz wave and generate hologram. For the insulating VO_2, incident wave is reflected by the lower gold antennas and the same hologram is generated with frequency doubling. Working frequencies of the designed holograms are 1.2 THz for metallic VO_2 and 1.9 THz for insulating VO_2. Due to the broadband performance under each state, the proposed metasurface can achieve holography within 1.0-2.1 THz. It is noteworthy that the generated holograms under two states of VO_2 remain entirely independent, and another metasurface that achieves frequency-multiplexed holograms is presented. Our design may have possible applications in holographic display and information encryption.

Keywords Metasurface, Hologram, Terahertz, VO_2

Electromagnetic (EM) waves are widely employed across numerous scientific fields, serving as our pivotal tools for comprehending and harnessing intricacies of the world. Within EM spectrum, terahertz waves occupy a distinctive position, delineated by wavelengths spanning from 3000 to 30 micrometers, which fall between microwave and infrared radiation. Nonetheless, people's comprehension of terahertz waves has historically lagged that of microwave and infrared technologies due to their idiosyncratic attributes. Yet, the 21st century has witnessed a burgeoning recognition of the significance of terahertz waves[1–3]. Meanwhile, terahertz waves have shown enormous potential in fields such as biomedicine[4,5] and wireless communication[6,7]. Terahertz waves exhibit an expanded broadband capacity and heightened spectrum utilization, thus emerging as a pivotal technology underpinning the evolution of sixth generation wireless systems[8,9]. However, the burgeoning complexity of application scenarios underscores an imperative for terahertz devices to embody attributes of diminutive size, multifaceted channel support, and broadband capability. This necessitates a paradigm shift towards the development of compact, multi-channel, and broadband-enabled terahertz devices to effectively navigate the exigencies of contemporary application landscapes.

In recent years, the limitations posed by the intrinsic complexity of natural materials have spurred interest in alternative approaches for precise control over terahertz waves. Metamaterials have emerged as a prominent artificial counterpart, garnering considerable attention owing to their exceptional EM properties. Through the deliberate design of specialized element arrays, metamaterials manifest unique EM responses, including but not limited to, negative refractive index phenomena[10]. However, due to its high loss and difficulty in production, metasurface as two-dimensional counterpart has become the preferred choice for people. In comparison to metamaterial counterparts, metasurfaces offer a compelling alternative, characterized by simplified structure, diminished loss, and enhanced cost-effectiveness. These attributes have significantly broadened the scope of their application domains. Metasurfaces wield the capacity to flexibly modulate various EM attributes such as polarization, amplitude, and phase[11–13]. This flexibility stems from the optimization of geometric parameters of the constituent meta-atoms. Through meticulous engineering, metasurfaces have achieved a myriad of functionalities including planar focusing[14–17], vortex beam[18,19], and broadband absorption[20,21]. Moreover, the augmentation of degrees of freedom has facilitated multi-channel reuse, thereby promoting the realization of multifunctional integration and enabling advanced applications such as information encryption[22]. In essence, metasurfaces epitomize a paradigm shift in EM manipulation, affording the unprecedented versatility and efficacy across diverse application landscapes.

Achievements of metasurfaces in holography are remarkable. Holography, by measuring amplitude as well as phase characteristics of wave, enables the presentation of three-dimensional images, thereby yielding more authentic and visually immersive effects. In contrast to conventional imaging techniques, holography boasts a richer detail. Holography requires high clarity and resolution, and metasurfaces are capable of precisely adjusting

School of Electronic Science and Engineering, Xiamen University, Xiamen 361005, China. ✉email: mw.zhuang@xmu.edu.cn; zhysong@xmu.edu.cn

amplitude as well as phase of EM waves. Therefore, metasurface holography has high application value. In recent years, this technology has made many breakthroughs. In 2013, Ni et al. introduced a novel structural paradigm to effectively generate holograms under visible light incidences, thus demonstrating a practical avenue for complex hologram production utilizing metasurfaces[23]. In 2015, Zheng et al. devised a geometric metasurface that substantially augmented diffraction efficiency of holograms engendered by circularly polarized incident light to an impressive 80%[24]. Concurrently, Wen et al. pioneered the integration of multiplexing concepts into holography, thereby enhancing the information capacity of metasurface[25]. Arbabi et al. refined the design methodologies pertaining to transmissive metasurfaces, thereby bolstering their efficacy in polarization and phase control[26]. In 2016, Liu et al. delved into the realm of anisotropic metasurfaces, unveiling their robust proficiency in manipulating terahertz waves[27]. Wang et al. presented a dielectric metasurface constructed from silicon nano-blocks, facilitating the simultaneous wavefront manipulation of three primary color lights[28]. In 2021, Bao et al. presented a strategy that breaks the traditional constraint of four degrees of freedom, resulting in a six-degree-of-freedom metasurface with the impressive performance in metasurface holography[29]. So far, there are still many breakthroughs in metasurface holography, which is one of the hot research areas related to metasurfaces.

Generally, once a metasurface sample is fabricated, it is challenging to alter its internal structural parameters. However, if methods can be developed to allow changes in physical properties of metasurface, its range of potential applications would be significantly broadened. Currently, the dynamic metasurface represents a frontier approach to achieving this goal[30,31]. Dynamic metasurface can modulate electromagnetic response through mechanisms such as electrical control[32]. The incorporation of phase-change materials (PCMs) is a promising method for realizing dynamic metasurfaces. PCMs are those that alter their state in response to external conditions without changing their fundamental structure. These materials exhibit distinct physical properties in different states, which is advantageous for multifunctional integration. Since the inception of metasurface research, many PCMs have been successfully applied to metasurfaces, including liquid crystal[33], doped semiconductor[34], GeSbTe[35], and graphene[36]. Among numerous materials, VO_2 stands out as a prominent PCM due to simple phase-change conditions and excellent performances. VO_2 is capable of reversible switching between metallic and insulating states. At room temperature, VO_2 exhibits insulating properties, whereas it behaves as a metal as temperature rises above 68 °C. Electrical conductivity of VO_2 differs by three orders of magnitude between two states, leading to significant changes in properties such as optical and electrical characteristics. Moreover, the transition of VO_2 states can be induced by electrical or light stimulation[37,38]. Extensive research has been conducted to harness unique properties of VO_2. In 2018, Ding et al. presented a broadband metasurface using VO_2, allowing it to switch from an absorber to a reflecting half-wave plate[39]. Two years later, Zhang et al. designed a multifunctional metasurface by using properties of VO_2, which enabled polarization state conversion and wide-range absorption[40]. Building upon this foundation, Liu and colleagues simultaneously utilized graphene and VO_2 to design a composite-configured dual-tunable absorption modulator[41]. These applications demonstrate the potential of PCMs like VO_2 and pave the way for new applications in dynamic modulation and tunable functional devices.

This study presents the design of VO_2 metasurfaces to achieve broadband holography for terahertz wave. The proposed metasurfaces can achieve holography within 1.0-2.1 THz. By exploiting the capacity to switch dielectric condition of VO_2, EM waves are redirected to different positions within the bilayer structure, enabling to generate holograms across distinct frequency bands. Notably, holograms produced in two states of VO_2 are found to be independent. Through careful alignment of center frequencies of imaging bands in both states, the metasurface demonstrates the capability for broadband holography. To optimize performance, four meta-atoms with phase difference of 90° are meticulously designed for each VO_2 state, ensuring comprehensive phase coverage and thereby enhancing the clarity and resolution of the resultant holograms. To elucidate operational principles of the designed metasurfaces, functional diagrams are provided in Fig. 1. In Fig. 1a, a square broadband hologram is designed with the center frequency of the imaging band at 1.2 THz for the metallic VO_2 and 1.9 THz for the insulating VO_2. Successful generation of broadband holograms at 1.0-2.1 THz is achieved. To illustrate the impact of VO_2 state switching and the independence of upper- and lower-layer images, a secondary sample is devised in Fig. 1b. This sample features a circular hologram for the metallic VO_2 and a hexagonal hologram for the insulating VO_2. Variation in temperature leads to corresponding alterations in the resulting holograms, further confirming the versatility and functionality of the proposed metasurface design.

Principle and design

The meta-atom is made of a bilayer structure. Each layer consists of three components including a designed antenna positioned in the upper section, a dielectric spacer in the middle, and a metallic substrate located in the lower section. This structure can form a metal-insulator-metal (MIM) space. Terahertz waves are capable of strongly engaging with MIM structure and being controlled by the specially designed antenna. VO_2 possesses excellent phase transition capabilities, allowing for the modulation of its conductivity by controlling temperature. Generally, at temperatures below 68 °C, VO_2 exhibits a conductivity of approximately 200 S/m, signaling an insulating state. In contrast, at temperatures above 68 °C, VO_2 exhibits a conductivity of approximately 3×10^5 S/m, signaling a metallic state. Working state of the upper MIM cavity is controlled by VO_2, enhancing control capabilities of meta-atoms over terahertz waves. For the metallic VO_2, substrate of the upper MIM structure can be approximated as metal substrate, thereby preventing transmission of incident wave and allowing only the upper MIM structure to function. Conversely, for the insulating VO_2, the influence of the upper MIM structure on incident wave can be neglected, effectively making only the lower MIM structure operational.

Figure 2 illustrates the proposed meta-atoms. Figure 2a presents a three-dimensional view of a localized meta-atom array, showcasing structural parameters utilized for achieving broadband terahertz holography. Period of $p = 100.0$ μm is used for meta-atom. The proposed meta-atom consists of two MIM structures. For the

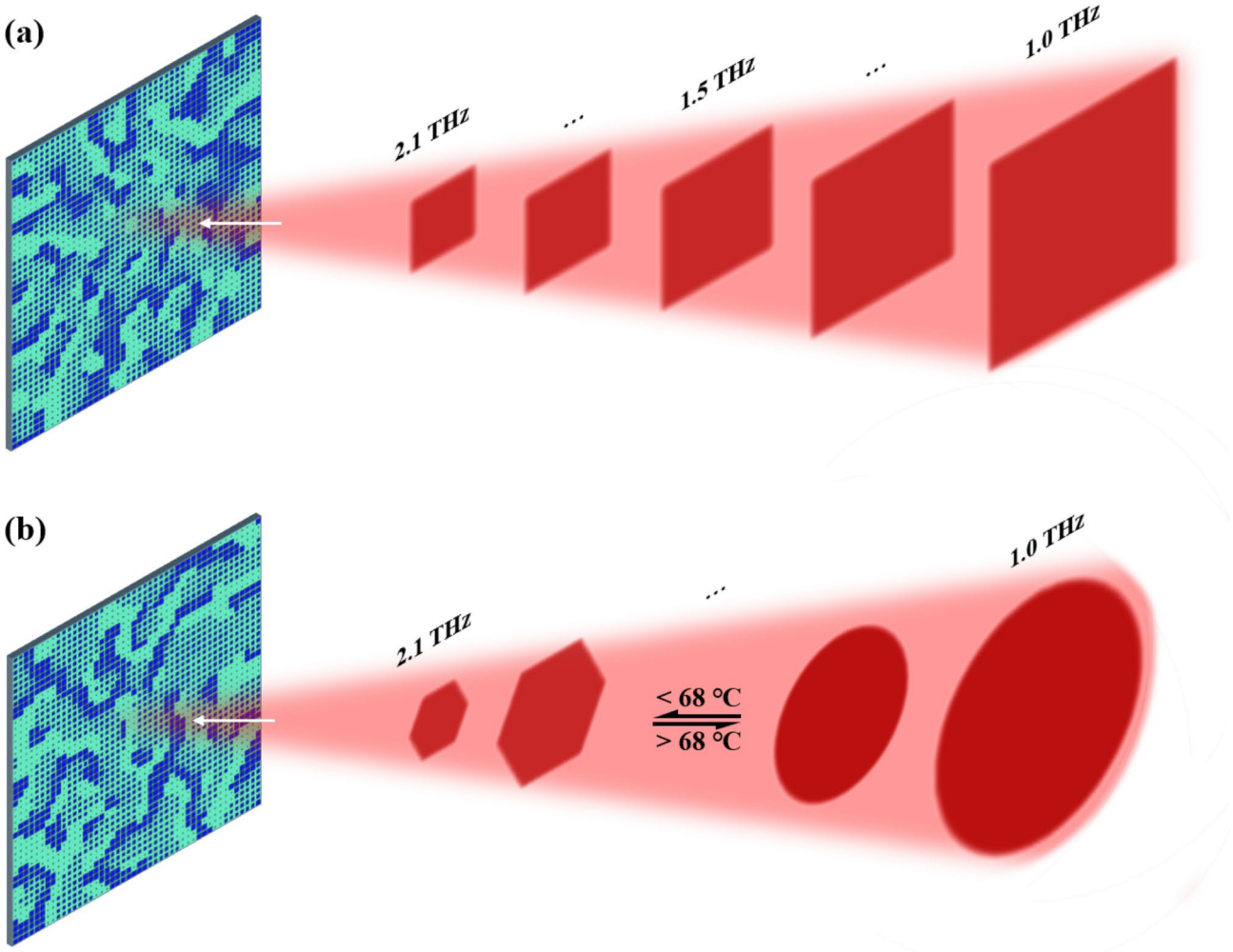

Fig. 1. Schematic diagrams of the designed metasurfaces, which achieves holography within 1.0-2.1 THz. (**a**) A square broadband hologram achieved by designing the same image for two states of VO_2. (**b**) Broadband holograms achieved by designing different images for two different states of VO_2.

upper MIM, the antenna is square-shaped, and both the antenna and the substrate are composed of VO_2. For the lower MIM, the antenna is cross-shaped, and both the antenna and the substrate are gold. The advantage of this isotropic bilayer structure lies in its ability to nearly eliminate cross polarization and coupling effect between each layer. The dielectric material for both MIM spacers is silicon dioxide (SiO_2). The thickness of VO_2 layers is $t_v = 1.0$ μm, while that of gold layers is $t_g = 0.5$ μm. The thickness of the upper SiO_2 spacer is $t_2 = 19.0$ μm, and that of the lower SiO_2 spacer is $t_1 = 10.0$ μm. These parameters are presented in Fig. 2b.

Within this bilayer structure, gold antenna is embedded in the dielectric spacer of upper MIM structure, and it is distributed centrally in square regions with the period of p/2. Gold antenna is isotropic with a length-to-width ratio of 5:1. Through simulation, four meta-atoms are achieved, and each exhibits a 90° phase difference as VO_2 is insulator. Four values of the length of gold antenna are $l_1 = 5.0$ μm, $l_2 = 29.8$ μm, $l_3 = 34.6$ μm, and $l_4 = 45.0$ μm. The upper VO_2 square antenna is positioned at the center of each meta-atom. Similarly, for the metallic VO_2, four meta-atoms are achieved and each exhibits a 90° phase difference. As illustrated in Fig. 2a, four values of the width of VO_2 square antenna are $w_1 = 12.0$ μm, $w_2 = 45.5$ μm, $w_3 = 51.6$ μm, and $w_4 = 74.0$ μm. Dielectric constant of SiO_2 is 3.85. Gold is a lossy metal with a conductivity of 4.561×10^7 S/m. Drude model is commonly used to describe dielectric constant of VO_2. Drude model is $\epsilon(\omega) = \epsilon_\infty - \frac{\omega_p^2(\sigma)}{\omega^2 + i\gamma\omega}$, where $\epsilon_\infty = 12$, $\omega_p^2(\sigma) = \frac{\sigma}{\sigma_0}\omega_p^2(\sigma)$ with $\sigma_0 = 3 \times 10^5\ S/m$, $\omega_p(\sigma_0) = 1.4 \times 10^{15}\ rad/s$, and $\gamma = 5.75 \times 10^{13} rad/s$ [42–44]. In simulation, the conductivity of VO_2 is $3 \times 10^5\ S/m$ $(200\ S/m)$ as it is metallic (insulating).

To achieve clear holograms, the proposed meta-atoms should exhibit 270° phase coverage with high reflectivity. Additionally, to enhance imaging efficiency, the number of meta-atom type should be kept to a minimum. Finite element method is employed in this study. Meta-atoms are arranged with periodic boundary conditions in x and y directions. Figure 3 illustrates simulation results of amplitudes and phases of meta-atoms

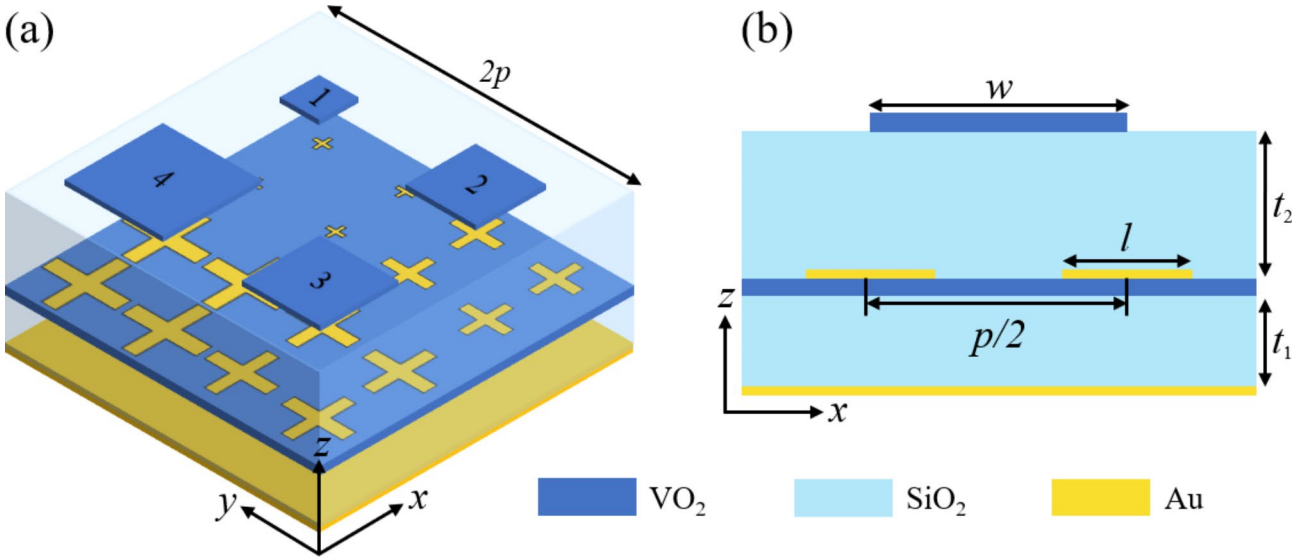

Fig. 2. (**a**) A three-dimensional view of a 2×2 array of meta-atoms, showcasing antenna parameters for two sets of antennas within two MIM cavities. The square VO_2 antennas have widths of $w_1 = 12.0$ μm, $w_2 = 45.5$ μm, $w_3 = 51.6$ μm, and $w_4 = 74.0$ μm, while dimensions of the cross-shaped gold antenna with an aspect ratio of 5:1 are given as $l_1 = 5.0$ μm, $l_2 = 29.8$ μm, $l_3 = 34.6$ μm, and $l_4 = 45.0$ μm. (**b**) The side view of the designed meta-atom, which is segmented into six components in two MIM structures.

under two states of VO_2. For the metallic VO_2 with $w_1 = 12.0$ μm, $w_2 = 45.5$ μm, $w_3 = 51.6$ μm, and $w_4 = 74.0$ μm as four suitable parameters, the desired effects are achieved by varying the width of the upper square VO_2 antennas. Conversely, for the insulating VO_2 with $l_1 = 5.0$ μm, $l_2 = 29.8$ μm, $l_3 = 34.6$ μm, and $l_4 = 45.0$ μm as four suitable parameters, the desired effects are attained by altering length and width of gold crosses. As depicted in Fig. 3a, amplitudes with four parameters are above 0.65 within 1.0-1.4 THz, and phase coverage with four parameters approximately meets 270°. We choose 1.2 THz as the center frequency for broadband imaging when VO_2 is metallic. In Fig. 3b, amplitudes are above 0.68 within 1.4–2.1 THz, and 90° phase difference is achieved between each meta-atom, indicating a broader bandwidth for achieving high-definition holography. We choose 1.9 THz as the center frequency for broadband imaging when VO_2 is insulating. Roles of two sets of parameters are independent of each other. For the metallic VO_2, the choice of the length of gold antenna doesn't affect characteristics of meta-atoms, while for the insulating VO_2, the choice of the width of VO_2 antenna is similarly inconsequential. It is worth mentioning that there is still room for optimization. Uniform quality of broadband holography is realized based on the 90° discrete phase coverage of meta-atoms. The different phase response in the frequency band should be optimized to be more parallel for better broadband performance. Optimization algorithm such as gradient descent method could be further used.

Results and discussion

The key to the design of metasurface hologram lies in determining phase distribution of the metasurface. This design process, known as phase retrieval, obtains corresponding phase distribution from a known amplitude distribution of image. This work adopts Gerchberg-Saxton (GS) algorithm for phase retrieval due to its suitability for computational technique, avoiding the need for complex setups and thus rendering phase search process highly efficient and accurate.

Based on GS algorithm, we design a terahertz metasurface comprising 46×46 meta-atoms for generating broadband holograms. Far-field monitors are placed with 0.1 THz interval at 1.0-2.1 THz. Image of the desired hologram in far field at 1.2 THz is illustrated in Fig. 4a. Based on this image, phase distribution of metasurface is obtained after iterations of GS algorithm in Fig. 4b. Within 1.0-1.4 THz, VO_2 is metal. When incident wave travels, only upper MIM structure is active for each meta-atom. This is because VO_2 substrate of upper MIM structure reflects the most part of incident wave, thereby preventing it from interacting with lower MIM structure. At this point, basic characteristics of metasurface are influenced by upper VO_2 antenna. Four designed square VO_2 antennas yield four different phase responses of reflected wave, serving as basic elements for phase distribution of the designed metasurface as VO_2 is metallic in Fig. 4b. Within 1.5–2.1 THz, VO_2 is insulator. At this stage, VO_2 structures in upper MIM do not reflect incident wave. Incident wave transmits through upper MIM, leaving only lower MIM structure active. At this point, basic characteristics of metasurface depend on lower cross-shaped gold antenna. Four designed cross-shaped gold antennas yield four different phase responses of reflected wave, serving as basic elements for phase distribution of the designed metasurface as VO_2 is insulating in Fig. 4b.

Simulated holograms are presented with the normalized intensity in Fig. 5. Figure 5a–e correspond to simulated results as VO_2 is metallic, while Fig. 5f–k correspond to simulated results as VO_2 is insulating. Imaging quality is optimized at center frequencies of 1.2 THz and 1.9 THz for these two frequency bands. Evaluation of hologram efficiency is carried out by calculating the far-field power ratio between the proposed metasurface and

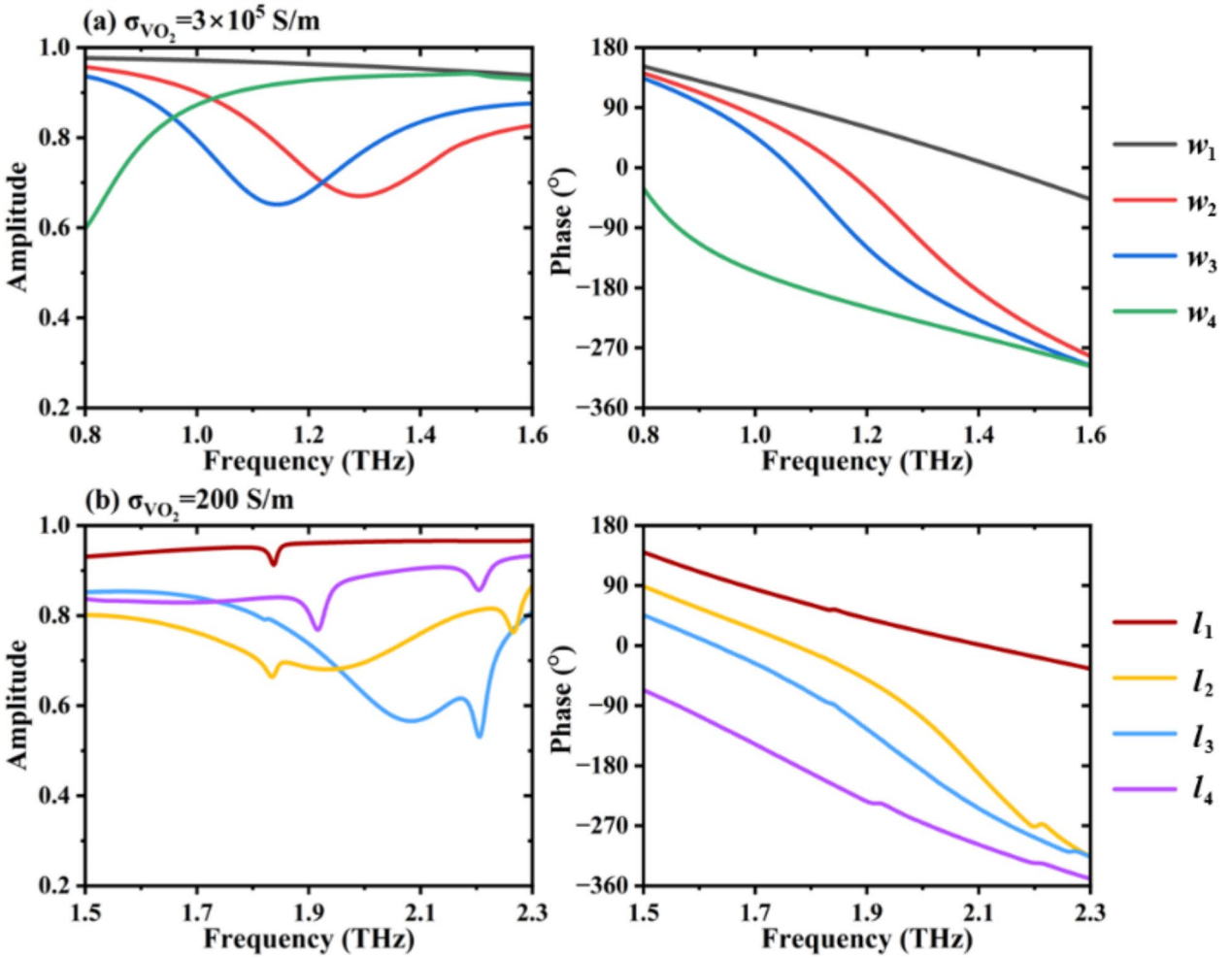

Fig. 3. Simulation results of basic characteristics of the designed meta-atoms for two states of VO_2. (**a**) For the metallic VO_2, simulated basic responses of the designed meta-atoms. (**b**) For the insulating VO_2, simulated basic responses of the designed meta-atoms.

a metal mirror. At 1.2 THz, hologram efficiency is 55.6%. Compared with the original image, root mean square error (RMSE) represents the quantified fidelity of hologram. Calculated RMSE for hologram is 0.058 at 1.2 THz, and it indicates higher fidelity. Holograms at other frequencies also exhibit sufficient clarity and integrity. However, the quality of holograms at 1.4 THz and 2.1 THz is somewhat inferior compared to others. It aligns with results in Fig. 3. Despite this, the produced holograms are relatively acceptable.

Our work also presents another metasurface to generate frequency-multiplexed broadband hologram, demonstrating the independence of two broadband terahertz holograms. In simulation, this metasurface comprises 46 × 46 meta-atoms, and simulation method and setup of far-field monitors are consistent with those used for the previous metasurface. In contrast to the previous case, holograms generated by this metasurface are circular when VO_2 is metallic, while those generated are hexagonal when VO_2 is insulating. We present images of holograms at center frequencies for both states of VO_2 in Fig. 6. Design method of hologram remains the same as that of the previous metasurface. We arrange square VO_2 antennas of upper MIM according to phase distribution in Fig. 6a and cross-shaped gold antennas of lower MIM according to phase distribution in Fig. 6b. This allows us to obtain two independent sets of holograms within 1.0-2.1 THz, which are solely controlled by the state of VO_2. Obtained holograms at 1.2 THz and 1.9 THz are displayed in Fig. 6. It is seen that the quality of both holograms is acceptable. Simulated hologram efficiencies are 55.7% and 85.9% for these two center frequencies, indicating the efficient performance. Compared with their original images, RMSEs are calculated as 0.053 and 0.052.

Furthermore, Fig. 7 shows obtained broadband holograms within 1.0-2.1 THz. Figure 7a–e represent simulated results when VO_2 is metallic, and Fig. 7f–k represent simulated results when VO_2 is insulating. It is evident that high-resolution holograms are produced within 1.0-2.1 THz even when image is altered. By varying the state of VO_2, it is possible to switch images across different frequency bands, thereby achieving frequency-multiplexed broadband holograms. This demonstrates the independence of the proposed broadband holograms.

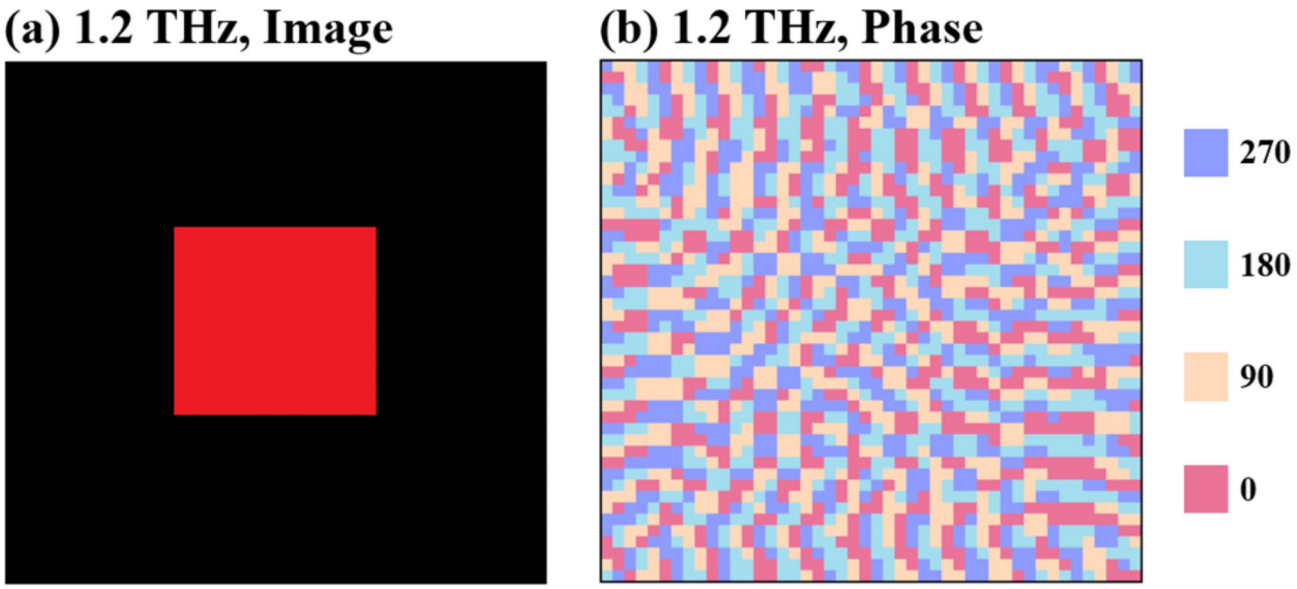

Fig. 4. (**a**) The ideal amplitude of far-field hologram at 1.2 THz. (**b**) The ideal phase distribution of the metasurface at 1.2 THz.

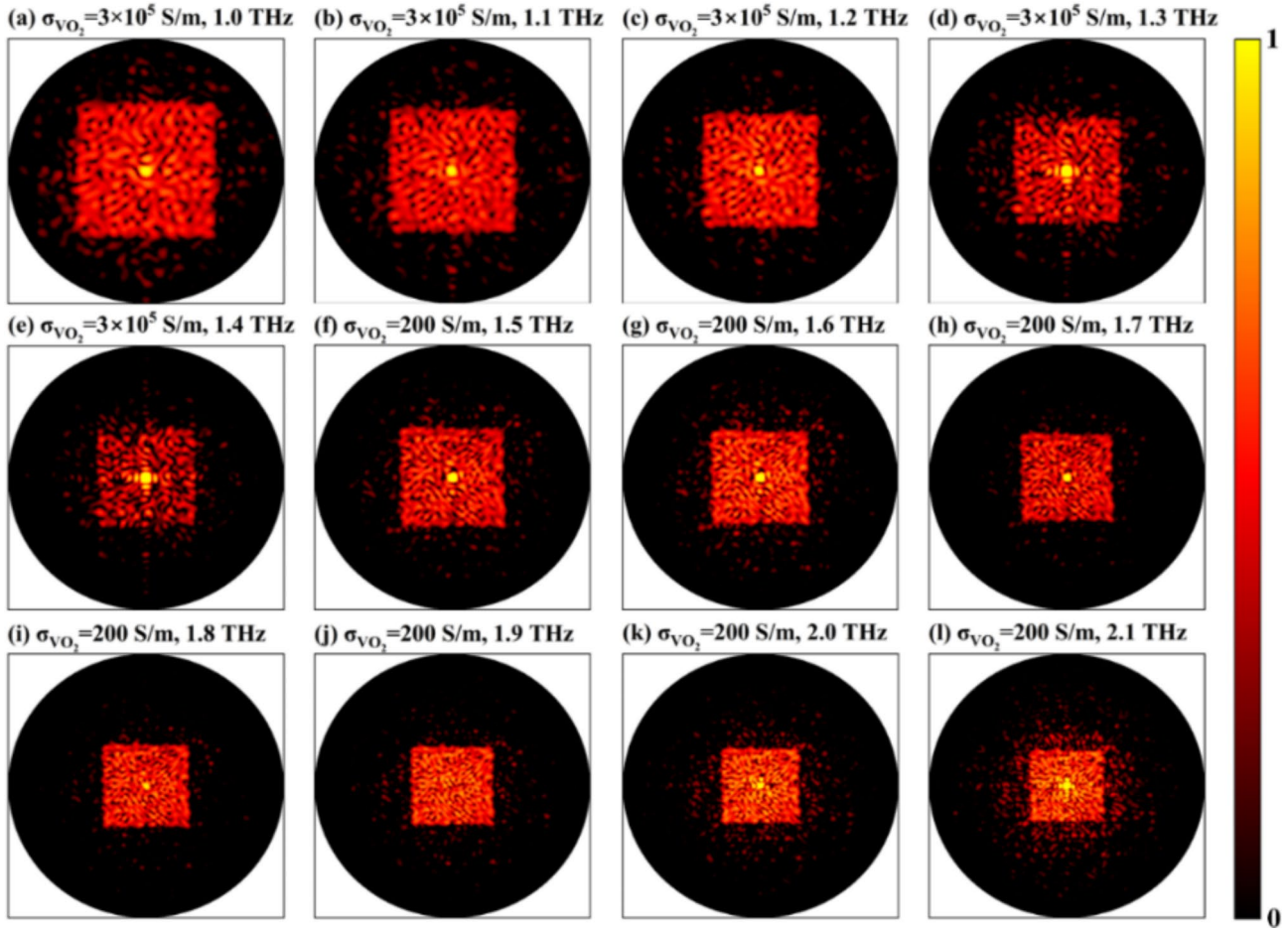

Fig. 5. The simulated holograms within 1.0-2.1 THz. (**a**–**e**) The obtained holograms as VO_2 are metallic. (**f**–**l**) The obtained holograms as VO_2 are insulating.

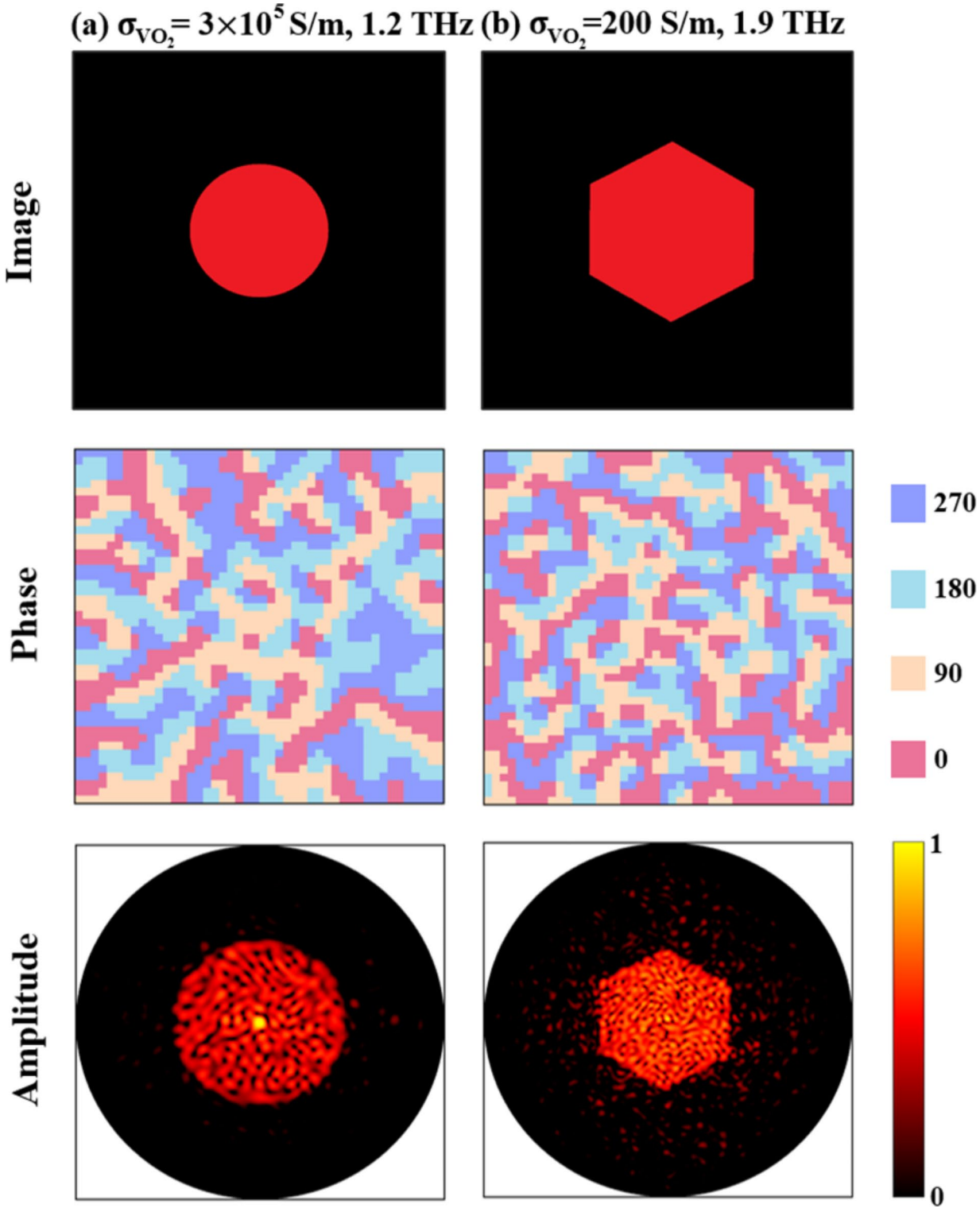

Fig. 6. (**a**) The ideal amplitude of far-field hologram, phase distribution of the metasurface, and actual amplitude of the circular hologram as VO_2 is metallic at 1.2 THz. (**b**) The ideal amplitude of far-field hologram, phase distribution of the metasurface, and actual amplitude of the hexagonal hologram as VO_2 is insulating at 1.9 THz.

Potential sample manufacturing and experimental measurement

The possible sample manufacturing steps for our designs mainly include lithography and deposition techniques. The lateral view of a single meta-atom in Fig. 8 provides a detailed representation of manufacturing process. Beginning with a SiO_2 substrate, a gold substrate and a SiO_2 spacer are deposited one after another. Subsequently,

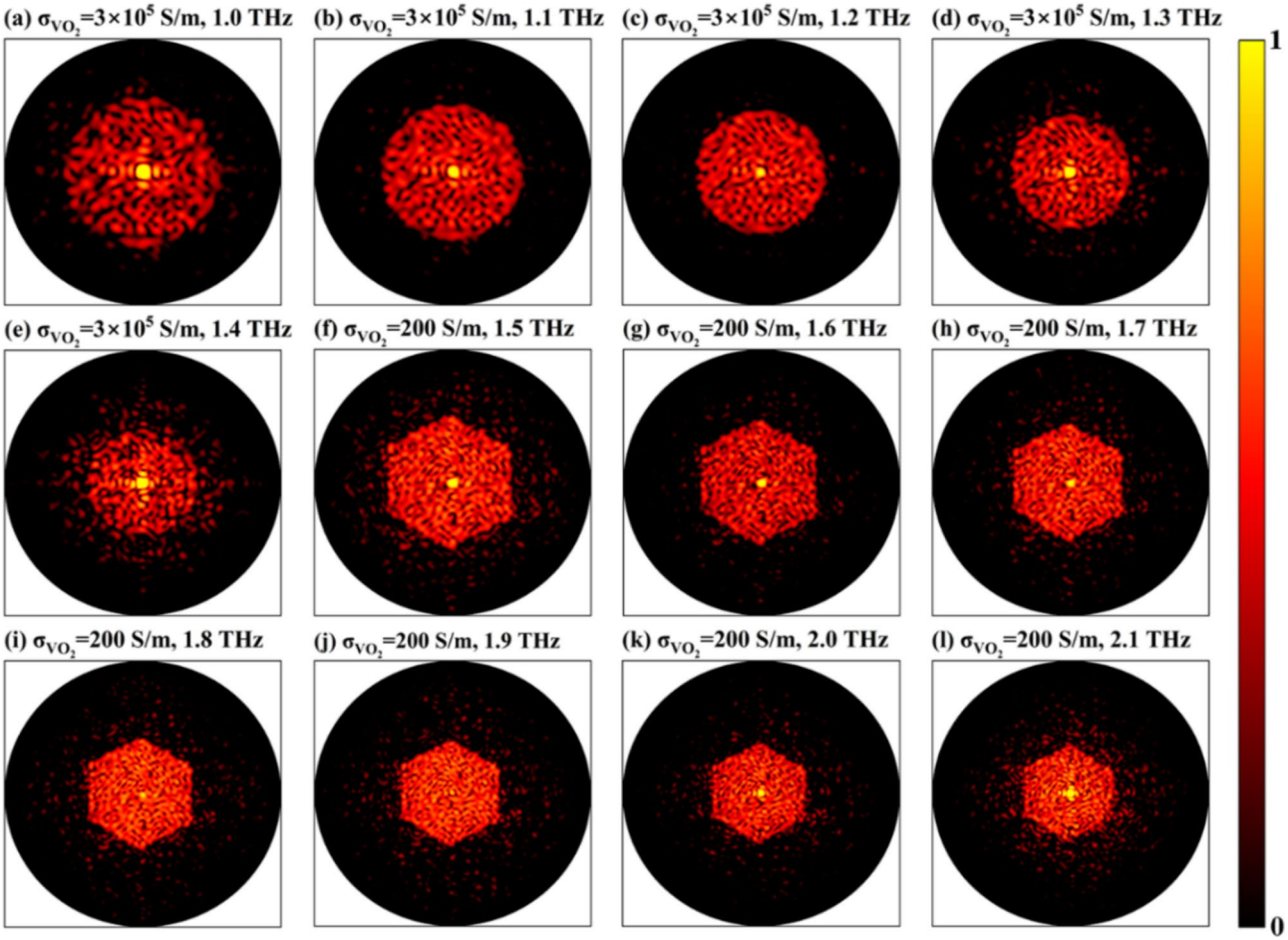

Fig. 7. Broadband terahertz frequency-multiplexed holograms. (**a**–**e**) The obtained circular holograms as VO_2 are metallic. (**f**–**l**) The obtained hexagonal holograms as VO_2 are insulating.

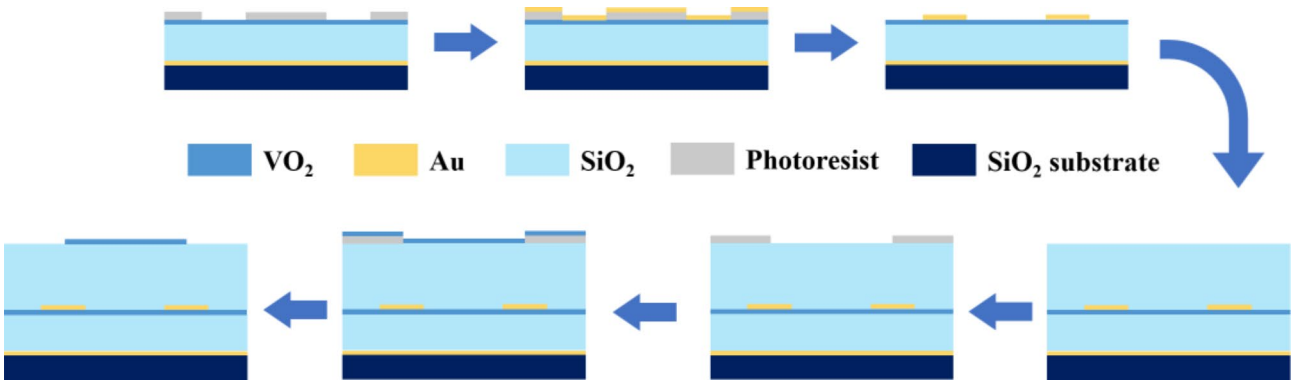

Fig. 8. Potential fabrication process of the proposed VO_2 metasurface.

a VO_2 film is sputtered onto the structure and annealed. Next, a layer of photoresist is spin-coated onto the surface and patterned using optical lithography to define the shape of cross-like patches for the lower MIM structure. A gold layer is then deposited over the patterned photoresist using electron beam evaporation. The lift-off process is employed to dissolve the photoresist, removing the excess gold and leaving behind the desired patterned gold patches. Then, another SiO_2 layer is deposited via electron beam evaporation. A second layer of photoresist is applied and shaped using optical lithography to define the square-shaped patches for the upper MIM structure. VO_2 is sputtered over the patterned photoresist, and another lift-off process is used to remove the photoresist and the extra VO_2 layer, leaving the final VO_2 patches. These remaining patches are then annealed to achieve the fabrication of the metasurface. Potential hologram measurement system is shown in Fig. 9. The

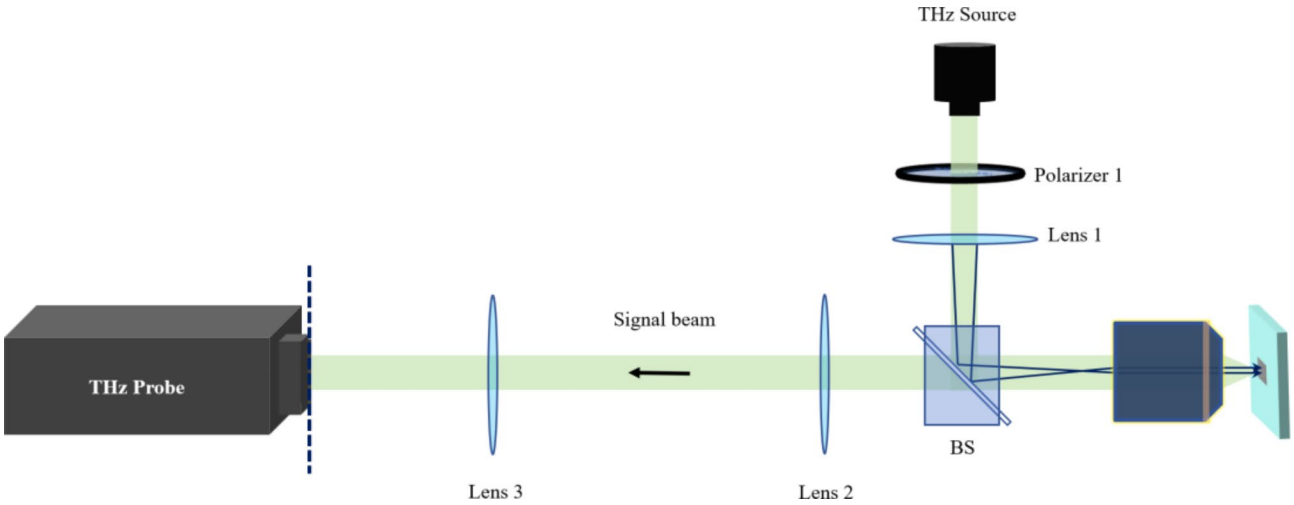

Fig. 9. Potential hologram measurement system.

entire system consists of a source, three lenses, an objective lens, a beam splitter, a linear polarizer, and a detector. In the measurement of far-field hologram, terahertz wave is emitted from the terahertz source and polarized by a linear polarizer. The rear plane of lens 1 and the objective lens are confocal, so that terahertz wave can be normally incident on the sample. The reflected signal is collected by the terahertz detector through confocal lenses 2 and 3, thus realizing the detection of hologram in the far field.

Conclusion

Utilizing a bilayer MIM structure based on VO_2, this work presents a novel approach for achieving broadband terahertz holography. For the metallic VO_2, the upper VO_2 square antennas reflect EM wave, yielding broadband holograms centered at 1.2 THz. Conversely, for the insulating VO_2, the lower gold cross-shaped antennas reflect terahertz wave, generating broadband holograms centered at 1.9 THz. Two frequency bands are closely adjacent by controlling the state transition of VO_2, allowing for the creation of broadband holograms within 1.0-2.1 THz. Furthermore, by altering the pattern of the hologram, the independence and adjustability of hologram are demonstrated under two states of VO_2. Compared to existing terahertz holography methods[45–48], our scheme has the limited channel number. However, our design offers higher holographic efficiency, polarization-insensitive control, and a broader bandwidth. There is potential for our designed VO_2 metasurface to be used in wavefront engineering[49] and holographic encryption[50].

Data availability

The datasets used and/or analysed during the current study available from the corresponding author on reasonable request.

Received: 28 November 2024; Accepted: 30 December 2024
Published online: 03 January 2025

References

1. Grady, N. K. et al. Terahertz metamaterials for linear polarization conversion and anomalous refraction. *Science* **340**(6138), 1304–1307 (2013).
2. Zhang, X. Q. et al. Terahertz surface plasmonic waves: A review. *Adv. Photonics*. **2**(1), 014001 (2020).
3. Liu, M., Yang, J., Du, Z., Xin, J. & Song, Z. Tripolarization-channel holograms generated by terahertz reflective bilayer-metasurface. *Opt. Lasers Eng.* **186**, 108763 (2025).
4. Ahmadivand, A., Gerislioglu, B., Ahuja, R. & Mishra, Y. K. Terahertz plasmonics: the rise of toroidal metadevices towards immunobiosensings. *Mater. Today* **32**, 108–130 (2020).
5. Yang, X. et al. Biomedical applications of terahertz spectroscopy and imaging. *Trends Biotechnol.* **34**(10), 810–824 (2016).
6. Huang, Y., Shen, Y. C. & Wang, J. Y. From terahertz imaging to terahertz wireless communications. *Engineering* **22**, 106–124 (2023).
7. Ma, J. J. et al. Security and eavesdropping in terahertz wireless links. *Nature* **563**(7729), 89–93 (2018).
8. Kildishev, A. V., Boltasseva, A. & Shalaev, V. M. Planar photonics with metasurfaces. *Science* **339**(6125), 1232009 (2013).
9. Leonhardt, U. Optical conformal mapping. *Science* **312**(5781), 1777–1780 (2006).
10. Smith, D. R., Pendry, J. B. & Wiltshire, M. C. K. Metamaterials and negative refractive index. *Science* **305**(5685), 788–792 (2004).
11. Yu, N. F. et al. Light propagation with phase discontinuities: Generalized laws of reflection and refraction. *Science* **334**(6054), 333–337 (2011).
12. Xu, Z., Yang, J. & Song, Z. Terahertz switchable metasurface for polarization conversion and hologram manipulation. *Opt. Lasers Eng.* **184**, 108641 (2025).
13. Yang, J., Xu, Z., Xin, J. & Song, Z. Temperature-assisted terahertz reconfigurable metasurface for multi-polarization holographic display and encryption. *Opt. Laser Technol.* **181**, 111968 (2025).
14. Wang, S. M. et al. A broadband achromatic metalens in the visible. *Nat. Nanotechnol* **13**(3), 227–232 (2018).
15. Avayu, O., Almeida, E., Prior, Y. & Ellenbogen, T. Composite functional metasurfaces for multispectral achromatic optics. *Nat. Commun.* **8**, 14992 (2017).

16. Chen, W. T., Zhu, A. Y., Sisler, J., Bharwani, Z. & Capasso, F. A broadband achromatic polarization-insensitive metalens consisting of anisotropic nanostructures. *Nat. Commun.* **10**, 355 (2019).
17. Arbabi, E. et al. MEMS-tunable dielectric metasurface lens. *Nat. Commun.* **9**, 812 (2018).
18. Devlin, R. C., Ambrosio, A., Rubin, N. A., Mueller, J. P. B. & Capasso, F. Arbitrary spin-to-orbital angular momentum conversion of light. *Science* **358**(6365), 896–900 (2017).
19. Guo, K., Xin, J. & Song, Z. Terahertz six-channel metasurface for the dynamic modulation of OAM. *J. Phys. D Appl. Phys.* **58**(6), 065109 (2025).
20. Kenney, M. et al. Octave-spanning broadband absorption of terahertz light using metasurface fractal-cross absorbers. *ACS Photonics* **4**(10), 2604–2612 (2017).
21. Aydin, K., Ferry, V. E., Briggs, R. M. & Atwater, H. A. Broadband polarization-independent resonant light absorption using ultrathin plasmonic super absorbers. *Nat. Commun.* **2**, 517 (2011).
22. Zheng, P. X. et al. Metasurface-based key for computational imaging encryption. *Sci. Adv.* **7**(21), eabg0363 (2021).
23. Ni, X. J., Kildishev, A. V. & Shalaev, V. M. Metasurface holograms for visible light. *Nat. Commun.* **4**, 2807 (2013).
24. Zheng, G. X. et al. Metasurface holograms reaching 80% efficiency. *Nat. Nanotechnol.* **10**(4), 308–312 (2015).
25. Wen, D. D. et al. Helicity multiplexed broadband metasurface holograms. *Nat. Commun.* **6**, 8241 (2015).
26. Arbabi, A., Horie, Y., Bagheri, M. & Faraon, A. Dielectric metasurfaces for complete control of phase and polarization with subwavelength spatial resolution and high transmission. *Nat. Nanotechnol.* **10**(11), 937–943 (2015).
27. Liu, S. et al. Anisotropic coding metamaterials and their powerful manipulation of differently polarized terahertz waves. *Light-Sci Appl.* **5**, e16076 (2016).
28. Wang, B. et al. Visible-frequency dielectric metasurfaces for multiwavelength achromatic and highly dispersive holograms. *Nano Lett.* **16**(8), 5235–5240 (2016).
29. Bao, Y. J., Wen, L., Chen, Q., Qiu, C. W. & Li, B. J. Toward the capacity limit of 2D planar Jones matrix with a single-layer metasurface. *Sci. Adv.* **7**(25), eabh0365 (2021).
30. Ding, F., Deng, Y. D., Meng, C., Thrane, P. & Bozhevolnyi, S. I. Electrically tunable topological phase transition in non-hermitian optical MEMS metasurfaces. *Sci. Adv.* **10**(5), eadl4661 (2024).
31. Meng, C., Thrane, P., Wang, C. S., Ding, F. & Bozhevolnyi, S. I. MEMS-tunable topological bilayer metasurfaces for reconfigurable dual-state phase control. *Optica* **11**(11), 1556–1566 (2024).
32. Ding, F., Meng, C. & Bozhevolnyi, S. I. Electrically tunable optical metasurfaces. *Photonics Insights* **3**(3), R07 (2024).
33. Li, S. Q. et al. Phase-only transmissive spatial light modulator based on tunable dielectric metasurface. *Science* **364**(6445), 1087–1090 (2019).
34. Shcherbakov, M. R. et al. Ultrafast all-optical tuning of direct-gap semiconductor metasurfaces. *Nat. Commun.* **8**, 17 (2017).
35. Cueff, S. et al. Reconfigurable flat optics with programmable reflection amplitude using lithography-free phase-change material ultra-thin films. *Adv. Opt. Mater.* **9**(2), 2001291 (2021).
36. Yao, Y. et al. Electrically tunable metasurface perfect absorbers for ultrathin mid-infrared optical modulators. *Nano Lett.* **14**(11), 6526–6532 (2014).
37. Wang, T. L., Zhang, H. Y., Zhang, Y., Zhang, Y. P. & Cao, M. Y. Tunable bifunctional terahertz metamaterial device based on Dirac semimetals and vanadium dioxide. *Opt. Express* **28**(12), 17434–17448 (2020).
38. Wong, A. M. H. & Eleftheriades, G. V. Perfect anomalous reflection with a bipartite Huygens' metasurface. *Phys. Rev. X* **8**(1), 011036 (2018).
39. Ding, F., Zhong, S. M. & Bozhevolnyi, S. I. Vanadium dioxide integrated metasurfaces with switchable functionalities at terahertz frequencies. *Adv. Opt. Mater.* **6**(9), 1701204 (2018).
40. Zhang, M., Zhang, J. H., Chen, A. P. & Song, Z. Y. Vanadium dioxide-based bifunctional metamaterial for terahertz waves. *IEEE Photonics J.* **12**(1), 4600109 (2020).
41. Liu, W. W. & Song, Z. Y. Terahertz absorption modulator with largely tunable bandwidth and intensity. *Carbon* **174**(15), 617–624 (2021).
42. Liu, M. et al. Terahertz-field-induced insulator-to-metal transition in vanadium dioxide metamaterial. *Nature* **487**(7407), 345–348 (2012).
43. Zhu, Y., Zhao, Y., Holtz, M., Fan, Z. & Bernussi, A. A. Effect of substrate orientation on terahertz optical transmission through VO_2 thin films and application to functional antireflection coatings. *J. Opt. Soc. Am. B.* **29**(9), 2373–2378 (2012).
44. Wang, S., Kang, L. & Werner, D. H. Hybrid resonators and highly tunable terahertz metamaterials enabled by vanadium dioxide (VO_2). *Sci. Rep.* **7**, 4326 (2017).
45. Bao, Y. J., Yan, J. H., Yang, X. G., Qiu, C. W. & Li, B. J. Point-source geometric metasurface holography. *Nano Lett.* **21**(5), 2332–2338 (2021).
46. Wu, T. et al. Spin-decoupled interference metasurfaces for complete complex-vectorial-field control and five-channel imaging. *Adv. Sci.* **9**(35), 2204664 (2022).
47. Wei, M. G. et al. Extended metasurface spin functionalities from rotation of elements. *Adv. Opt. Mater.* **10**(24), 2201975 (2022).
48. Wang, Y., Yao, Z. Y., Cui, Z. J., Sun, G. C. & Zhang, D. C. Orbital angular momentum multiplexing holography based on multiple polarization channel metasurface. *Nanophotonics* **12**(23), 4339–4349 (2023).
49. Huang, S. H. et al. Microcavity-assisted multi-resonant metasurfaces enabling versatile wavefront engineering. *Nat. Commun.* **15**(1), 9658 (2024).
50. Song, Q. H. et al. Printing polarization and phase at the optical diffraction limit: Near- and far-field optical encryption. *Nanophotonics* **10**(1), 697–704 (2021).

Author contributions

Jiayu Zhao, Runxuan Zhang, Sicheng Cao, Mingwei Zhuang, and Zhengyong Song: Data curation, Investigation, Writing - original draft. Mingwei Zhuang and Zhengyong Song: Conceptualization, Funding acquisition, Supervision, Writing - review & editing.

Funding

This work is supported by Fujian Provincial Natural Science Foundation of China (2024J01053) and Natural Science Foundation of Xiamen (3502Z202473013).

Declarations

Competing interests

The authors declare no competing interests.

Additional information

Correspondence and requests for materials should be addressed to M.Z. or Z.S.